AIP | Applied Physics Letters

Enhanced Raman scattering and photoluminescence of Bi3.25La0.75Ti3O12 nanotube arrays for optical and ferroelectric multifunctional applications

J. Z. Zhang, M. J. Han, Y. W. Li, Z. G. Hu, and J. H. Chu

Citation: Appl. Phys. Lett. **101**, 081903 (2012); doi: 10.1063/1.4747218
View online: http://dx.doi.org/10.1063/1.4747218
View Table of Contents: http://apl.aip.org/resource/1/APPLAB/v101/i8
Published by the American Institute of Physics.

Enhanced Raman scattering and photoluminescence of $Bi_{3.25}La_{0.75}Ti_3O_{12}$ nanotube arrays for optical and ferroelectric multifunctional applications

J. Z. Zhang (张金中), M. J. Han (韩美杰), Y. W. Li (李亚巍), Z. G. Hu (胡志高),[a)]
and J. H. Chu (褚君浩)
Key Laboratory of Polar Materials and Devices, Ministry of Education, Department of Electronic Engineering, East China Normal University, Shanghai 200241, People's Republic of China

(Received 23 April 2012; accepted 6 August 2012; published online 21 August 2012)

Raman scattering enhancement has been observed from highly ordered ferroelectric $Bi_{3.25}La_{0.75}Ti_3O_{12}$ nanotube (BLT-NT) arrays prepared by a template-assisted method. Scattering enhancement factor which is the ratio of average Raman intensity per molecule for nanostructure and film is evaluated to be about 92, 257, and 623 corresponding to the outer diameters of 50, 100, and 200 nm, respectively. The phenomena can be attributed to unique surface, microstructure, grain size, and tensile stress in the curved nanotube walls. These results indicate that BLT-NT arrays are suitable for fabricating multifunctional devices due to remaining good ferroelectricity. © *2012 American Institute of Physics*. [http://dx.doi.org/10.1063/1.4747218]

Over the past decade, researches on perovskite ferroelectric nanostructure have advanced significantly, while the focus has mainly been on synthesis to date.[1–4] Template-assisted synthesis of micro- or nano-tubes and wires is a versatile and inexpensive technique for fabricating ferroelectric structures. Size, shape, and structural properties of the assembly are simply controlled by adopting various templates such as alumina membranes, porous silicon, and polycarbonate membranes.[5–9] Recently, there are some attempts to study ferroelectric, piezoelectric, and dielectric properties of ferroelectric nanotubes for improving storage density of random access memory.[10,11] Fortunately, some measurements show well-saturated hysteresis loops in ferroelectric nanostructure at room temperature.[12–14] For example, remanent polarization ($2P_r$) and coercive field ($2E_c$) of ferroelectric $Pb(Zr, Ti)O_3$ nanotubes are about 3 $\mu C/cm^2$ and 172 kV/cm, respectively.[12] On the other hand, bismuth (Bi)-layered perovskite $Bi_{3.25}La_{0.75}Ti_3O_{12}$ (BLT) is another attractive ferroelectric material because BLT compounds are lead free which have high dielectric constant and remanent polarization, as well as fatigue free.[15–17] However, there are few studies on optical and ferroelectric properties of BLT nanotube (NT) arrays. Moreover, Raman scattering and photoluminescence (PL) from ferroelectric BLT-NTs have been rarely reported. Thus, it is necessary to further study growth and physical properties of BLT-NT structures in order to develop promising devices.

In this letter, we present enhanced Raman scattering, PL, and ferroelectric properties of highly ordered BLT-NT arrays with length of 60 μm and outer diameters of 50, 100, and 200 nm prepared using a template-assisted method, which integrates a sol-gel technique with a spin-coating process. A definition of Raman scattering enhancement factor for NT material has been proposed. Intensity of PL emission located at about 2.3 eV is enhanced significantly, and ferroelectric properties of BLT-NT arrays can be well remained.

Analytically pure bismuth nitrate, lanthanum nitrate, and titanium butoxide were used as starting materials for (Bi, La, and Ti)-precursor solution. Nanoporous anodic aluminum oxide (AAO) templates were prepared by two-step anodization process [insets of Figs. 1(a)–1(c)]. Before fabrication of BLT-NT arrays, the AAO templates were fixed on $Pt/Ti/SiO_2/Si$ substrates and then immersed in the solution. The spinning was performed using a spinner rotated at a speed of 3500 rpm for 30 s to avoid the presence of a film surface on BLT-NT arrays. In order to obtain single perovskite phase, the templates with the precursor inside were subsequently heated in air at 675 °C for 10 min. Finally, the as-prepared samples were wet chemical etched in 1 M NaOH solution for about 150 min to remove the AAO templates. Then, BLT-NT arrays were washed by de-ionized water to remove remnant NaOH. For comparison, the as-deposited BLT films were heated with the same temperature as that of BLT-NTs.

Morphology and chemical composition of BLT-NT arrays with diameters of 50, 100, and 200 nm were characterized by a field emission scanning electron microscopy (FESEM: Philips XL30FEG) with an energy dispersive x-ray analyzer. Microstructure of BLT-NTs was investigated by x-ray diffraction (XRD) using a Ni filtered Cu Kα radiation source (D/MAX-2550 V, Rigaku Co.) and a transmission electron microscopy (TEM: JEOL JEM-2100F). Raman spectra were recorded by a micro-Raman spectrometer (Jobin-Yvon LabRAM HR 800 UV) with a 488 nm laser line, and photoluminescence spectra were measured by the same instrument using a He-Cd laser ($\lambda = 325$ nm, power: 20 mW). Ferroelectric hysteresis loops of BLT-NT arrays were recorded by a ferroelectric test system (Precision Premier II: Radiant Technologies Inc.). Piezoresponse force microscopy (PFM) loops were obtained using a Bruker dimension icon atomic force microscope with a doped diamond conductive probe (Bruker DDESP-10). It should be pointed out that all optical and electrical measurements were carried out at room temperature.

Figs. 1(a)–1(c) show the typical scanning electron microscopy (SEM) images of BLT-NTs with diameters of

[a)]Author to whom correspondence should be addressed. Electronic mail: zghu@ee.ecnu.edu.cn. Tel.: +86-21-54345150. Fax: +86-21-54345119.

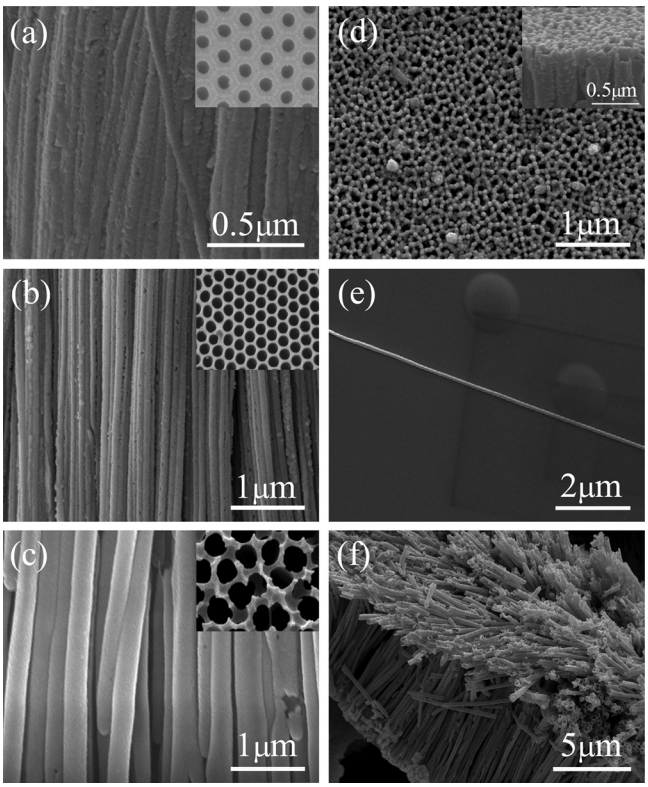

FIG. 1. Cross-sectional SEM images of BLT-NT arrays with outer diameters of about (a) 50, (b) 100, and (c) 200 nm and insets are the corresponding AAO templates. (d) Top and side view of 200 nm-diameter BLT-NT array. (e) A single high aspect ratio tube and (f) a cluster of BLT nanotubes.

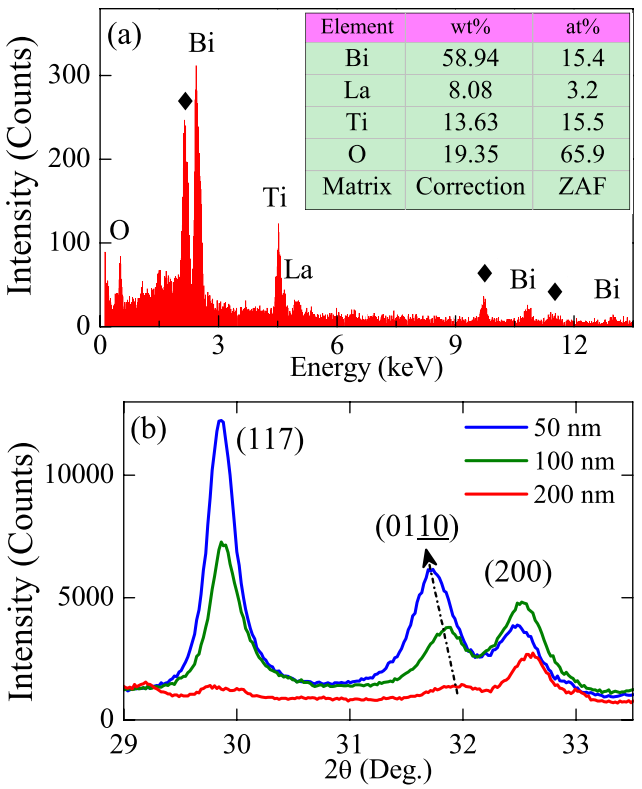

FIG. 2. (a) An EDS spectrum acquired from as-prepared BLT-NTs confirms that the nanotubes consist of Bi, La, Ti, and O elements with a stoichiometric $Bi_{3.25}La_{0.75}Ti_3O_{12}$ composition. The lozenge symbol (◆) indicates the peaks of Au element originated from sample preparation. (b) XRD patterns of ferroelectric perovskite BLT-NTs with outer diameters of 50, 100, and 200 nm. Arrow shows the variation trend of the (200) peak with increased the diameter.

50, 100, and 200 nm. It indicates that the nanotubes are smooth and the outer diameters are consistent with the corresponding pore size of the AAO templates. It means that the templates have been completely removed in the wet etching process. The top- and side-view SEM images of BLT-NT array show that the tubes are open-ended and hollow [Fig. 1(d) and the inset]. As an example, a sectioned single high aspect ratio tube and a cluster of BLT-NTs are presented in Figs. 1(e) and 1(f), respectively. The energy dispersive x-ray spectroscopy (EDS, using an EDS spectrometer attached to SEM) was performed on pristine BLT-NT array to quantitatively analyze the chemical composition as shown in Fig. 2(a). It is clear that the nanotubes consist of Bi, La, Ti, and O elements and the atomic ratio is 15.4:3.2:15.5:65.9, which is approximate to an ideal stoichiometric value. There are no traces of Na contamination from NaOH etchant and Al element, which confirms that the AAO templates have been completely dissolved. It should be noted that the Au element, indicated by the symbol (◆), is originated from sample preparation for SEM measurement. The XRD patterns show that there are diffraction peaks (117), (0110), (200), etc. (JCPDS card, No. 80-2143), which suggest that as-prepared BLT-NT arrays are polycrystalline with single perovskite phase [Fig. 2(b)]. The (200) peak position shifts towards a lower degree side with decreased outer diameter due to a higher surface tension. As increasing tube diameter, the degree of *a*-orientation is improved, in which direction spontaneous polarization is much larger than that in the *c*-direction at room temperature.[16,19] Therefore, BLT-NT arrays are superior to film structure in the application of ferroelectric random-access memories.

Microstructure of BLT-NT arrays was further characterized by transmission electron microscopy (TEM). An apparent hollow morphology was testified by the transparency between the intermediary areas and edges of the tube-like samples (Fig. 3). The wall thicknesses of the nanotubes are about 8, 12, and 14 nm, which corresponds to the outside diameter of 50, 100, and 200 nm, respectively [Figs. 3(a)–3(c)]. As an example, Fig. 3(e) illustrates the wall thickness (14 nm) of the nanotubes with a outer diameter of about 200 nm. The thickness of tube wall increases with the outside diameter because a larger nanopore can accommodate more precursor solution. In addition, the wall thickness can be controlled by repeating the cycle of sol filling, coating, and annealing. A high-resolution TEM image taken on the wall of a BLT-NT with outer diameter of 200 nm shows that the grain size is tens of nanometers. The insets are the selected area electron diffraction (SAED) patterns with diffraction rings and distinct BLT spots, such as (020), (00$\underline{1}$0), and (02$\underline{1}$0) ([$\bar{1}$00] zone axis patterns), which are taken from the nanotubes with diameters of 100 and 200 nm, respectively. It is found that BLT-NTs are polycrystalline (though they may have a single-crystalline fraction) and occupy perovskite phase with lattice parameters of $a \approx b = 0.57 \pm 0.03$ and $c = 3.31 \pm 0.05$ nm. These values are slightly larger than those of films ($a \approx b = 0.54 \pm 0.01$ and $c = 3.30 \pm 0.01$ nm) fabricated by the same method.[20] As compared to the results from the XRD analysis, slight discrepancy may be attributed to surface tension of the BLT-NTs.[21,22]

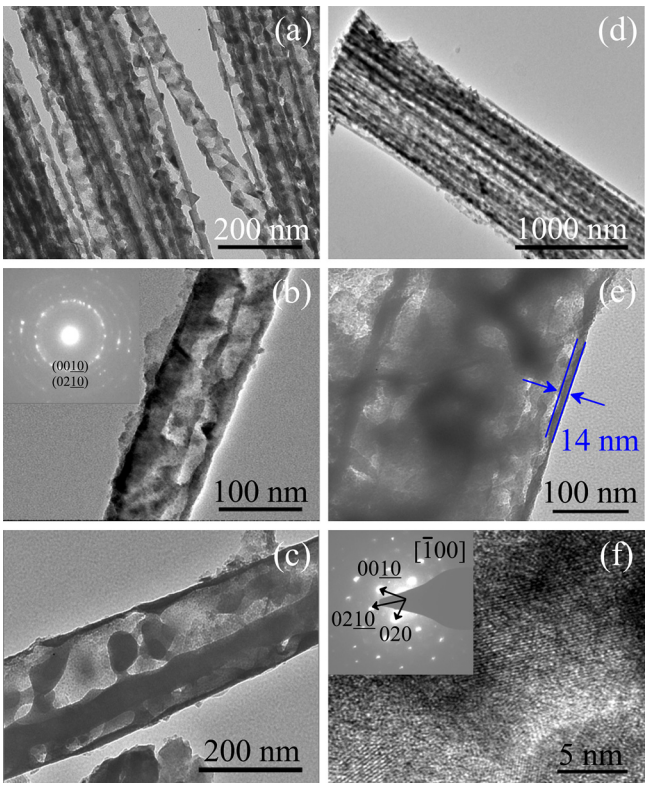

FIG. 3. TEM images of BLT-NT arrays with outer diameters of about (a) 50, (b) 100, and (c) 200 nm. (d) A bundle of 100 nm-diameter BLT nanotubes. (e) An individual BLT-NT with a wall thickness of about 14 nm. (f) A high-resolution image of a BLT-NT with perovskite grains and the insets are the corresponding SAED patterns.

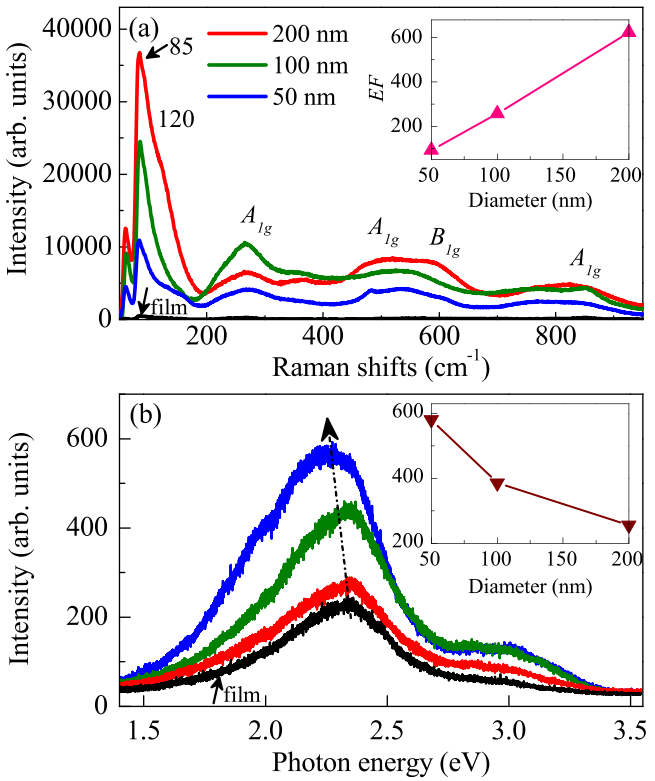

FIG. 4. (a) Enhanced Raman spectra of varied diameter BLT-NTs and film. Inset shows Raman scattering enhancement factors as a function of nanotube diameter. (b) Enhanced PL spectra of varied BLT-NTs and film and the inset shows the peak intensity (~2.3 eV) as a function of diameter. Arrow shows the changing trend of the PL peak position.

Based on microstructural information obtained from the SEM, XRD, and TEM analysis, a possible nucleation mechanism of BLT-NTs can be proposed. Hydrophilic pore walls of AAO templates are positively charged due to hydrated ions $Al(H_2O)_n^{3+}$, $Al(H_2O)_n(OH)^{2+}$ and/or $Al(H_2O)_n(OH)_2^{+}$ (n is natural number). At the same time, the acidic (Bi, La, and Ti)-precursor (PH ≈ 4) is composed of Bi^{3+}, La^{3+}, and Ti^{4+} cations. Therefore, homogeneous nucleation would be preferred because these cations repel the pore walls.[18] The grain growth follows the classical Ostwald-ripening, namely bigger crystals grow at the expense of smaller ones.

Recently, it has been determined that $Bi_4Ti_3O_{12}$ belongs to the monoclinic system with space group $B1\ a1$, which is a commensurate modulation of the nonpolar orthorhombic parent $Fmmm$. It is predicted to have 24 first-order Raman-active modes ($6A_g + 2B_{1g} + 8B_{2g} + 8B_{3g}$) at the Γ point of Brillouin zone.[23] Fig. 4(a) shows Raman scattering of as-prepared BLT-NT arrays and film. It is interesting to observe that Raman intensities of BLT-NT arrays with varied diameters are much stronger than that of BLT film and increase with increased the outer diameter. Generally, intensity of Raman scattering is dependent of differential scattering cross section $d^2\sigma/(d\Omega d\omega)$. The scattering photons are located in the solid angle ($d\Omega$) and frequency ($d\omega$) ranges.[24] BLT-NT arrays and films are prepared with the same (Bi, La, and Ti)-precursor solution under the same condition. The physical properties should be similar and can be reasonably compared. It was reported that BLT film has a smooth surface with a root-mean-square roughness of about 8 nm from atomic force microscopy images.[20] On the other hand, enhanced Raman scattering is sensitive to surface morphology of sample. Therefore, it is reasonable to adopt BLT film as reference to give a definition for enhancement factor. In order to quantitatively evaluate enhanced Raman scattering phenomena under a certain experimental conditions, an enhancement factor (EF) is defined.[25] The EF of BLT-NT arrays can be written as

$$EF = A \cdot \frac{I_{NT}/N_{NT}}{I_F/N_F}, \tag{1}$$

where A is a constant associated with inherent physical quantities of a material such as mole mass and effective electron mass. I_{NT} and I_F are experimental Raman intensities of the nanotube and film, respectively. N_{NT} and N_F are the average number of molecules in scattering volume of the nanotube and film, respectively. Here, parameter A approaches unity and $N_{NT}/N_F = \pi(R^2 - r^2)/(2\sqrt{3}R^2)$. Therefore, the EF is the ratio of average Raman intensity per molecule for nanotube and film materials. According to the definition, the EF of BLT-NT arrays with outer diameters ($R = 50$, 100, and 200 nm) and inner diameters ($r = 42$, 88, and 186 nm) are of about 92, 257, and 623 [inset of Fig. 4(a)]. Optical enhancements of the composite systems can be explained using Maxwell-Garnett and more sophisticated effective medium theories.[26] The electromagnetic fields can be localized in the inter- and intra-tube regions. Amplification of both incident laser field and scattered Raman field is enhanced through the

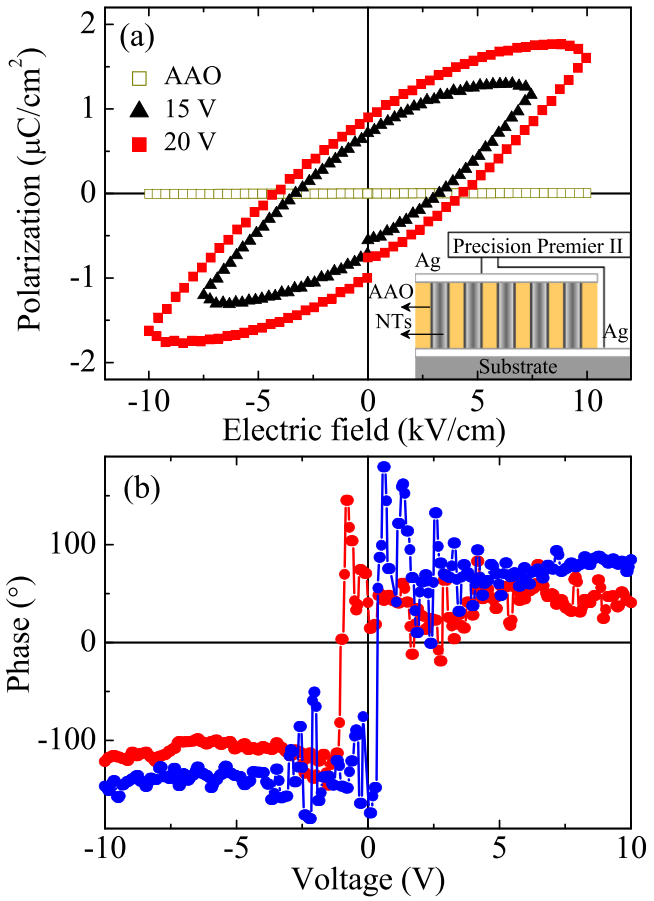

FIG. 5. (a) Polarization-electric field (*P-E*) of AAO templates (hollow square) and BLT-NT array in 200 nm-nanopore AAO template. Insets show the corresponding capacitor devices and ferroelectric measurement setup. (b) Piezoelectric phase hysteresis loop of BLT-NTs with outer diameter of 200 nm.

interaction with the surface and microstructure of nanotube arrays. Therefore, enhanced Raman intensity may be due to unique surface, microstructure, grain size, and tensile stress in the curved nanotube walls. This specifically enhanced Raman scattering features enable the demonstration of multi-gate logic devices and other optoelectronic devices with electronic input and optical output.[27,28]

On the other hand, PL characterization shows a broadening and intense emission band located at about 2.3 eV. It indicates that the intensity increases with decreased tube diameter and it is stronger than that of BLT film [Fig. 4(b)]. This phenomenon can be well explained by PL quantum yield theory:[29] $\eta_R \equiv (dm/dt)_{radiative}/(dm/dt)_{total} = \tau_{NR}/(\tau_{NR} + \tau_R)$, where m is the number of photons emitted in a given time t, τ_R and τ_{NR} are the radiative and non-radiative lifetime of the transition from excited states to ground ones. The PL quantum yield increases with decreased outer diameter because sharp angled surface and lattice defects shorten the radiative lifetime and/or prolong the non-radiative lifetime.[30] The enhanced PL observed in BLT-NT material may origin from sharp angled surface, oxygen vacancies, and dangling bonds on the surface of nanotubes.

For investigating ferroelectric properties of BLT-NT arrays, polarization-electric field (*P-E*) hysteresis loops of BLT films and nanotubes in the AAO template were measured. The BLT films with the thickness of about 450 nm show well-saturated hysteresis loops. Under a maximum application electric field of about 220 kV/cm, the values of $2P_r$ and $2E_c$ are 20.5 $\mu C/cm^2$ and 146 kV/cm, respectively (not shown). On the other hand, the *P-E* loops of BLT-NT arrays are not saturated because of low applied electric field and existence of leakage current. In order to separate effects of the AAO templates on ferroelectric properties of BLT-NT arrays, the *P-E* loops of a AAO template were measured and marked by the symbol (hollow square) [Fig. 5(a)]. It is found that the AAO templates do not exhibit ferroelectric properties. It means that ferroelectricity of BLT-NTs in the AAO templates is mainly originated from BLT-NT arrays themselves. Moreover, Fig. 5(b) shows piezoelectric phase hysteresis loop of BLT-NTs with outer diameter of 200 nm from PFM measurements. The square phase hysteresis loop reflects piezoresponse property of BLT-NTs. There is a shift of the curve to negative bias voltage, which may be caused by surface and space charge. In addition, a decrease at high electric field is ascribed to a consequence of field-induced lattice hardening which is typical for perovskite piezoelectrics.[31]

In summary, with a facile template process, we provide the preparation of free-standing BLT-NT arrays with outer diameters of 50, 100, and 200 nm on $Pt/Ti/SiO_2/Si$ substrates. Enhanced Raman scattering of the nanotubes are evaluated to be about 92, 257, and 623 corresponding to the outer diameters of 50, 100, and 200 nm, respectively. The enhancements can be attributed to unique surface, microstructure, grain size, and tensile stress in the curved nanotube walls. Moreover, as-prepared BLT-NT arrays present remarkable PL emission and good ferroelectric features. These results are valuable for the achievement of optical and ferroelectric multifunctional devices.

J. Z. Zhang is grateful to Qian Yu, Wenlei Yu, Zhenni Zhan, and Yuanyuan Liao for technical supports. This work was financially supported by the Major State Basic Research Development Program of China (Grant No. 2011CB922200), the Natural Science Foundation of China (Grant Nos. 11074076, 60906046, and 61106122), the Projects of Science and Technology Commission of Shanghai Municipality (Grant Nos. 11520701300, 10DJ1400201, and 10SG28), and the Program for Professor of Special Appointment (Eastern Scholar) at Shanghai Institutions of Higher Learning.

[1]J. F. Scott, H. J. Fan, S. Kawasaki, J. Banys, M. Ivanov, A. Krotkus, J. Macutkevic, R. Blinc, V. V. Laguta, P. Cevc, J. S. Liu, and A. L. Kholkin, Nano Lett. **8**, 4404 (2008).
[2]Y. Nakayama, P. J. Pauzauskie, A. Radenovic, R. M. Onorato, R. J. Saykally, J. Liphardt, and P. Yang, Nature (London) **447**, 1098 (2007).
[3]S. S. Nonnenmann, O. D. Leaffer, E. M. Gallo, M. T. Coster, and J. E. Spanier, Nano Lett. **10**, 542 (2010).
[4]H. Han, Y. Kim, M. Alexe, D. Hesse, and W. Lee, Adv. Mater. **23**, 4599 (2011).
[5]W. Liu, X. H. Sun, H. W. Han, M. Y. Li, and X.-Z. Zhao, Appl. Phys. Lett. **89**, 163122 (2006).
[6]Y. Luo, I. Szafraniak, N. D. Zakharov, V. Nagarajan, M. Steinhart, R. B. Wehrspohn, J. H. Wendorff, R. Ramesh, and M. Alexe, Appl. Phys. Lett. **83**, 440 (2003).
[7]F. D. Morrison, L. Ramsay, and J. F. Scott, J. Phys.: Condens. Matter **15**, L527 (2003).
[8]Y. Wang and G. Z. Cao, J. Mater. Chem. **17**, 894 (2007).
[9]B. Im, H. Jun, K. H. Lee, S.-H. Lee, I. K. Yang, Y. H. Jeong, and J. S. Lee, Chem. Mater. **22**, 4806 (2010).
[10]C. H. Ahn, K. M. Rabe, and J.-M. Triscone, Science **303**, 488 (2004).

[11]X. H. Zhu, Z. G. Liu, and N. B. Ming, J. Mater. Chem. **20**, 4015 (2010).
[12]J. Kim, S. A. Yang, Y. C. Choi, J. K. Han, K. O. Jeong, Y. J. Yun, D. J. Kim, S. M. Yang, D. Yoon, H. Cheong, K.-S. Chang, T. W. Noh, and S. D. Bu, Nano Lett. **8**, 1813 (2008).
[13]D. Zhou, H. S. Gu, Y. M. Hu, Z. L. Qian, Z. L. Hu, K. Yang, Y. N. Zou, Z. Wang, Y. Wang, J. G. Guan, and W. P. Chen, J. Appl. Phys. **107**, 094105 (2010).
[14]W. Cai, X. M. Lu, H. F. Bo, Y. Kan, Y. Y. Weng, L. Zhang, X. B. Wu, F. Z. Huang, L. M. Eng, J. S. Zhu, and F. Yan, J. Appl. Phys. **110**, 052004 (2011).
[15]B. H. Park, B. S. Kang, S. D. Bu, T. W. Noh, J. Lee, and W. Jo, Nature (London) **401**, 682 (1999).
[16]H. N. Lee, D. Hesse, N. Zakharov, and U. Gosele, Science **296**, 2006 (2002).
[17]Y. Shimakawa, Y. Kubo, Y. Tauchi, H. Asano, T. Kamiyama, F. Izumi, and Z. Hiroi, Appl. Phys. Lett. **79**, 2791 (2001).
[18]L. Shi, C. J. Pei, Y. M. Xu, and Q. Li, J. Am. Chem. Soc. **133**, 10328 (2011).
[19]H. Irie, M. Miyayama, and T. Kudo, J. Appl. Phys. **90**, 4089 (2001).
[20]J. Z. Zhang, X. G. Chen, K. Jiang, Y. D. Shen, Y. W. Li, Z. G. Hu, and J. H. Chu, Dalton Trans. **40**, 7967 (2011).
[21]Y. Zheng, C. H. Woo, and B. Wang, J. Phys.: Condens. Matter **20**, 135216 (2008).
[22]T. Shimada, X. Wang, Y. Kondo, and T. Kitamura, Phys. Rev. Lett. **108**, 067601 (2012).
[23]J. M. Perez-Mato, P. Blaha, K. Schwarz, M. Aroyo, D. Orobengoa, I. Etxebarria, and A. Garcia, Phys. Rev. B **77**, 184104 (2008).
[24]J. Neugebauer, M. Reiher, C. Kind, and B. A. Hess, J. Comput. Chem. **23**, 895 (2002).
[25]E. C. Le Ru, E. Blackie, M. Meyer, and P. G. Etchegoin, J. Phys. Chem. C **111**, 13794 (2007).
[26]A. Campion and P. Kambhampati, Chem. Soc. Rev. **27**, 241 (1998).
[27]E. H. Witlicki, C. Johnsen, S. W. Hansen, D. W. Silverstein, V. J. Bottomley, J. O. Jeppesen, E. W. Wong, L. Jensen, and A. H. Flood, J. Am. Chem. Soc. **133**, 7288 (2011).
[28]Y. B. Zheng, J. L. Payton, C.-H. Chung, R. Liu, S. Cheunkar, B. K. Pathem, Y. Yang, L. Jensen, and P. S. Weiss, Nano Lett. **11**, 3447 (2011).
[29]G. S. Hong, S. M. Tabakman, K. Welsher, H. L. Wang, X. R. Wang, and H. J. Dai, J. Am. Chem. Soc. **132**, 15920 (2010).
[30]X. Wu, T. Ming, X. Wang, P. N. Wang, J. F. Wang, and J. Y. Chen, ACS Nano **4**, 113 (2010).
[31]H. Zheng, J. Wang, S. E. Lofland, Z. Ma, L. Mohaddes-Ardabili, T. Zhao, L. Salamanca-Riba, S. R. Shinde, S. B. Ogale, F. Bai, D. Viehland, Y. Jia, D. G. Schlom, M. Wuttig, A. Roytburd, and R. Ramesh, Science **303**, 661 (2004).